

# SYMMETRY ENERGY: FROM NUCLEAR MATTER TO FINITE NUCLEI

V. M. Kolomietz and A. I. Sanzhur

Institute for Nuclear Research, NAS of Ukraine, Prospekt Nauky 47, 03680 Kyiv, Ukraine

## Abstract

We suggest a particular procedure of derivation of the beta-stability line and isotopic symmetry energy. The behavior of the symmetry energy coefficient  $b(A, N - Z)$  is analyzed. We redefine the surface tension coefficient and the surface symmetry energy for an asymmetric nuclear Fermi-liquid drop with a finite diffuse layer. Following Gibbs-Tolman concept, we introduce the equimolar radius at which the surface tension is applied. The relation of the nuclear macroscopic characteristics like surface and symmetry energies, Tolman length, etc. to the bulk properties of nuclear matter is considered. The surface-to-volume symmetry energy ratio for several Skyrme-force parametrizations is obtained.

## INTRODUCTION

Many static and dynamic features of nuclei are sensitive to the symmetry energy and the isospin degrees of freedom. The basic characteristics of isovector giant and isobar analog resonances [1], the isoscaling in nuclear fission and multifragmentation [2, 3, 4, 5, 6, 7, 8, 9] depend significantly on the isospin effects. The symmetry energy is also a key element for the derivation of the nuclear stability valley. The nuclear  $\beta$ -stability is determined by the balance of the isotopic symmetry,  $E_{\text{sym}}$ , and the Coulomb,  $E_C$ , energies. However the extraction of both  $E_{\text{sym}}$  and  $E_C$  from the nuclear binding energy is not a simple problem because of their complicate dependency on the mass number  $A = N + Z$  in finite nuclei with  $N$  neutrons and  $Z$  protons [10]. The standard procedure of extraction of the symmetry energy from a fit of mass formula to the experimental binding energies [11] is not free from ambiguities and does not allow one to separate the symmetry energy into the volume and surface contributions directly. In the present work, to study the structure of the  $\beta$ -stability line and both  $E_{\text{sym}}$  and  $E_C$  energies we use a particular procedure which is based on the dependence of the isospin shift of neutron-proton chemical potentials  $\Delta\lambda(X) = \lambda_n - \lambda_p$  on the asymmetry parameter  $X = (N - Z)/(N + Z)$  for nuclei beyond the  $\beta$ -stability line. This procedure allows us to represent the results for the  $A$ -dependence of the  $\beta$ -stability line and both energies  $E_{\text{sym}}$  and  $E_C$  in a transparent way, which can be easily used for the extraction of the smooth volume and surface contributions as well as their shell structure. Note also that our procedure of extraction of all values  $E_C(A)$  and  $E_{\text{sym}}$  is partly model independent, that is, the theoretical models for calculations of the nuclear binding energy as well as the nucleon distributions are not involved. We only assume the commonly used parabolic dependence of the symmetry energy on the asymmetry parameter  $X$ . Due to the charge invariance of the nuclear forces this assumption is well justified for small values of  $X$ . A similar approach based on the isobaric multiplet mass equation [12] was used in Ref. [13] to study the Coulomb parameter within the modern nuclear mass model WS3.

The nucleus is a two component, charged system with a finite diffuse layer. This fact specifies a number of various peculiarities of the nuclear surface and symmetry energies: dependency on the density profile function, non-zero contribution to the surface symmetry energy, connection to the nuclear incompressibility, etc. The additional refinements appear due to the quantum effects arising from the smallness of nucleus. In particular, the curved interface creates the curvature correction to the surface energy  $E_S$  and the surface part of symmetry energy  $E_{\text{sym}}$  of order  $A^{1/3}$  and can play the appreciable role in small nuclei as well as in neck region of fissionable nuclei. The presence of the finite diffuse layer in nuclei creates the problem of the correct definition of the radius and the surface of tension for a small drop with a diffuse interface. Two different radii have to be introduced in this case [14, 15]: the equimolar radius  $R_e$ , which gives the actual size of the corresponding sharp-surface droplet, and the radius of tension  $R_s$ , which derives, in particular, the capillary pressure. Below we will address this problem to the case of two-component nuclear drop. In general, the presence of the curved interface affects both the bulk and the surface properties. The curvature correction is usually negligible in heavy nuclei. However, this correction can be important in some nuclear processes. For example the yield of fragments at the nuclear multifragmentation or the probability of clusterization of nuclei from the freeze-out volume in heavy ion collisions [16]. In both above mentioned processes, small nuclei necessarily occur and the exponential dependence of the yield on the surface tension [17] should cause a sensitivity of both processes to the curvature correction. Moreover the dependency of the curvature interface effects on the isotopic asymmetry of small fragments can significantly enhance (or suppress) the yields of

neutron rich isotopes. In this paper we analyze of the interface effects in an asymmetric nuclear Fermi-liquid drop with a finite diffuse layer. We follow the ideology of the extended Thomas-Fermi approximation (ETFA) with effective Skyrme-like forces combining the ETFA and the direct variational method with respect to the nucleon densities, see Ref. [18]. The surface and symmetry energies were widely studied earlier taking into consideration also the finite surface thickness and the curvature corrections [19, 20, 21, 22, 23, 24]. Note also the applications of the ETFA with the Skyrme-type interactions to the studies of the nuclear bulk, surface and symmetry properties, see e.g. Refs. [25, 26, 27, 28]. In order to formulate proper definition for the drop radius, we use the concept of the dividing surface, originally introduced by Gibbs [14]. Following the Gibbs method, which is applied to the case of two component system, we introduce the superficial (surface) density as the difference (per unit area of dividing surface) between actual number of particles  $A$  and the number of bulk,  $A_V$ , and neutron excess,  $A_{-,V}$ , particles which a drop would contain if the particle densities were uniform.

## STRUCTURE OF $\beta$ -STABILITY LINE AND SYMMETRY ENERGY

Considering the asymmetric nuclei with a small asymmetry parameter  $X = (N - Z)/A \ll 1$ , the total energy per nucleon  $E/A$  can be represented in the following form of  $A, X$ -expansion,

$$E/A = e_0(A) + b(A)X^2 + E_C(X)/A, \quad (1)$$

where  $e_0(A)$  includes both the bulk and the surface energies,  $b(A)$  is the symmetry energy coefficient,  $E_C(X)$  is the total Coulomb energy

$$E_C(X)/A = e_C(A)(1 - X)^2. \quad (2)$$

Using the derivation of the chemical potential  $\lambda_q$  ( $q = n$  for a neutron and  $q = p$  for a proton)

$$\lambda_n = \left( \frac{\partial E}{\partial N} \right)_Z, \quad \lambda_p = \left( \frac{\partial E}{\partial Z} \right)_N, \quad (3)$$

one can write the condition of nuclear  $\beta$ -stability in the following form

$$\lambda_n - \lambda_p = 2 \frac{\partial(E/A)}{\partial X} \Big|_A = 0. \quad (4)$$

The beta-stability line  $X^*(A)$  is directly derived from Eqs. (1), (2) and (4) as

$$X^*(A) = \frac{e_C(A)}{b(A) + e_C(A)} \quad (5)$$

We point out that for finite nuclei, the beta-stability condition  $\lambda_n - \lambda_p = 0$  is not necessary fulfilled explicitly because of the subshell structure in the discrete spectrum of the single particle levels near the Fermi energy for both the neutrons and the protons. Note also that, strictly speaking, the  $\beta$ -decay is forbidden if  $|\lambda_n - \lambda_p| < m_e c^2$ , where  $m_e$  is the electron (positron) mass, i.e., in general, the condition  $\lambda_n - \lambda_p = 0$  for  $\beta$ -stability is too strong and we can expect more smooth behavior of  $X^*(A)$  than the one given by Eq. (5).

Along the  $\beta$ -stability line, the binding energy per particle is given by

$$E^*/A = e_0(A) + b(A)X^{*2} + E_C(X^*)/A, \quad (6)$$

where the upper index “\*” indicates that the corresponding quantity is determined by the variational conditions (5) taken for fixed  $A$  and  $X = X^*$  on the beta-stability line. For any given value of mass number  $A$ , the binding energy per nucleon  $E/A$  can be extended beyond the beta-stability line as

$$E/A = E^*/A + b(A)(X - X^*)^2 + \Delta E_C(X)/A, \quad (7)$$

where  $\Delta E_C(X) = E_C(X) - E_C(X^*)$ . The symmetry energy coefficient  $b(A)$  contains the  $A$ -independent bulk term,  $b_V$ , and the  $A$ -dependent surface contribution,  $b_S A^{-1/3}$ ,

$$b(A) = b_V + b_S A^{-1/3}. \quad (8)$$

In general, the surface symmetry energy includes also the high order curvature correction  $\propto A^{-2/3}$  [18].

Using Eq. (7), one can establish an important relation for the chemical potentials  $\lambda_q$  beyond the beta-stability line. Namely, for the fixed particle number  $A$ , we obtain from Eqs. (1), (6) and (5) the following relation

$$\Delta\lambda(A, X)/4 = (\lambda_n - \lambda_p)/4 = \frac{1}{2} \frac{\partial(E/A)}{\partial X} \Big|_A = [b(A) + e_C(A)] X - e_C(A). \quad (9)$$

On the other hand, the shift  $\Delta\lambda(A, X)$  of the neutron-proton potentials can be evaluated numerically within the accuracy of  $\sim 1/A^2$  using for the quantity of  $\partial(E/A)/\partial X$  in Eq. (9) the experimental values of the binding energy per nucleon  $\mathcal{B}(N, Z) = -E(N, Z)/A$ . Namely,

$$\frac{\partial(E/A)}{\partial X} \Big|_A = \frac{A}{4} [\mathcal{B}(N-1, Z+1) - \mathcal{B}(N+1, Z-1)]. \quad (10)$$

Since the difference (10) is taken for  $\Delta Z = -\Delta N = 2$ , the pairing effects do not affect the resulting accuracy. It was shown in Ref. [29] that the linear dependence of  $\Delta\lambda(A, X)$  given by Eq. (9) at fixed particle number  $A = \text{const}$  is reproduced quite well experimentally. This fact allows one to extract the values of  $b(A)$ ,  $e_C(A)$ , and  $X^*$  for a given mass number  $A$  with acceptable accuracy.

Using Eqs. (9) and (10), we have evaluated the "experimental" values of quantities  $X^*(A)$  and  $b(A)$  along the Periodic Table of the Elements. From the beta-stability condition  $\Delta\lambda(A, X) = 0$  and Eqs. (9) and (10) we can derive the asymmetry parameter  $X^*(A)$ . In Fig. 1, we have plotted the obtained "experimental" value of  $X^*(A)$  (solid dots). The  $\beta$ -stability line  $X^*(A)$  can be also evaluated theoretically using an appropriate equation of state (EOS). In our numerical calculations we have used the EOS from the extended Thomas-Fermi approximation (ETFA) with Skyrme forces [30]. The result of the typical microscopic calculation of  $X^*(A)$  within the extended Thomas-Fermi approximation with Skyrme forces SLy230b is shown in Fig. 1 as the dashed line. The numerical results presented in Fig. 1 depends slightly only on the specific choice of Skyrme force parametrization. For comparison the dotted line in Fig. 1 shows the analogous result for Skyrme forces SkM.

The thin solid line in Fig. 1 was obtained by use the phenomenological Green-Engler formula [31]

$$X^*(A) = \frac{0.4 A}{A + 200}. \quad (11)$$

The "experimental" curve (solid dots)  $X^*(A)$  in Fig. 1 shows the non-monotonic (sawtooth) shape as a function of the mass number  $A$ . This behavior is the consequence of subshell structure of the single particle levels near the Fermi surface for both the neutrons and the protons. Because of this subshell structure, the Fermi levels for protons and neutrons can coincide (such a coincidence is the condition for the  $\beta$ -stability) by chance only creating the non-monotonic behavior of  $X^*(A)$ . Note that the non-monotonic subshell structure of the  $\beta$ -stability line is transparently discovered for the curve  $X^*(A)$  only, i.e., for  $A$ -dependency of  $X^*$ . The traditional representation of  $\beta$ -stability line as  $Z(N)$ -dependency does not allow one to observe this phenomenon. The reason is that the shell oscillations appear against the small asymmetry parameter  $X^*(A)$  which is close to zero. For the same reason the value of  $X^*(A)$  requires more rigorous description than  $Z(N)$ .

We point out also that the traditionally used beta-stability line  $Z(N)$  is given for a discrete set of the asymmetry parameter  $X$  and the mass number  $A$  which obey the condition  $|\Delta\lambda(A, X)| < m_e c^2$ . Under this condition the beta-stable nuclei represent rather eroded area than line as compared to the more tight definition  $\Delta\lambda(A, X) = 0$ . In Fig. 1 we have plotted the discrete points of the beta-stability line  $Z(N)$  as the open circles. Each open circle in Fig. 1 corresponds to the stable isotope of maximum abundance for a certain value of charge number  $Z$ . As seen from Fig. 1, there is a correlation between the locations of solid dots and open circles. The location of the  $\beta$ -stability line defined by the condition  $\Delta\lambda(A, X) = 0$  (solid dots) is obviously less scattered over the plot area, especially for light nuclei. In practical sense, the  $A$ -dependent  $\beta$ -stability line  $X^*(A)$  is useful to extract the Coulomb energy parameter  $e_C(A)$  and the symmetry energy  $b(A)$  from the experimental data by use the chemical potential shifts  $\Delta\lambda(A, X)$ , see e.g. Eq. (9).

To show the origin of the subshell oscillations of  $X^*(A)$  more transparently, we will consider the sequence of the nucleon magic numbers [32]: 8, 20, 28, 50, 82 and 126. From this sequence one should expect special behavior of the  $X^*(A)$  nearby the following values of mass number  $A = N + Z$ : 28 (20+8), 48 (28+20), 78 (50+28), 132 (82+50) and 208 (126+82). The "experimental" beta-stability line (solid dots in Fig. 1) has the local maxima at mass numbers 24 (13+11), 48 (26+22), 84 (48+36), 133 (79+54) and 208 (126+82). We can see that mass numbers of local maxima in Fig. 1 does not exactly follow double magic numbers. Nevertheless, one can state that, at least approximately, there exists the correlation between the positions of maxima of sawtooth function  $X^*(A)$  and double magic mass numbers.

The Coulomb energy parameter  $e_C(A)$  in Eq. (9) can be easily evaluated for a given proton density distribution independently on the nuclear  $NN$ -interaction. In the simplest case, assuming a sharp proton distribution and neglecting the contribution from the quantum exchange term, one obtains  $e_C(A) =$

$0.15Ae^2/R_C \propto A^{2/3}$ , where  $R_C$  is the charge (Coulomb) radius of nucleus. In general, both the finite diffuse layer and the quantum exchange contributions must be taken into account. The last fact leads to more complicate  $A$ -dependence of  $e_C(A)$ . To extract such an actual  $A$ -dependency of the Coulomb parameter  $e_C(A)$  which includes both above mentioned contributions, we will consider the values of the chemical potential shift  $\Delta\lambda(A, X)$  at the fixed neutron excess,  $A_- = N - Z = AX$  and the different particle numbers  $A$ . As seen from Eq. (9), for the zero's neutron excess  $A_- = 0$  the value of  $\Delta\lambda(A, X)$  is not affected by the symmetry energy  $b$  and it is completely determined by  $e_C(A)$ . Due to this fact, for nuclei with  $A_- = 0$  the Coulomb parameter  $e_C(A)$  can be evaluated precisely including all corrections caused by the finite diffuse layer, the quantum exchange effects, etc. The Coulomb parameter  $e_C(A)$  can be represented by the smooth function

$$e_C(A) = C_1 A^{2/3} + C_2 A^{1/3} \quad (12)$$

with  $C_1 = 0.207$ ,  $C_2 = -0.174$  obtained using the fit to all available "experimental" data with  $A_- = 0$ . The use of Eq. (9) for the shift  $\Delta\lambda(X)$  at fixed  $A$  allows us to determine the Coulomb parameter  $e_C(A)$  for the whole region of mass number covered by experimental data. This was earlier done in Ref. [29] where the Coulomb parameter  $e_C(A)$  was roughly estimated as  $e_C(A) \approx 0.17A^{2/3}$ . However, more precise evaluation is complicated because of the strong shell oscillations at  $e_C(A)$ . In contrast, the data for  $e_C(A)$  obtained from (9) at fixed  $A_- = 0$  do not show much shell structure. This fact is also supported by results of Ref. [13].

Note that the actual value of the Coulomb parameter  $e_C(A)$  can deviate from its extrapolation given by Eq. (12) for heavy nuclei with  $X \neq 0$ . This deviation is caused by the fact that the proton distribution radius  $R_C$  is slightly dependent on the neutron excess ("neutron skin") in asymmetric nuclei. The origin of such dependency is the polarization effect. Namely, the saturation bulk density decreases with  $X$  for neutron-rich nuclei where more neutrons are pushed off to the "neutron skin" involving also the protons and increasing thereby the radius of proton distribution. Such kind of polarization effect of the neutron excess on the proton distribution can be estimated evaluating the  $X$ -dependency of the bulk density in asymmetric nuclei [33, 34, 35]. The estimation made in [30] shows that the influence of the neutron excess on the Coulomb radius  $R_C$  is negligible in asymmetric nuclei with  $X \ll 1$  and the extrapolation formula (12) for the Coulomb energy parameter  $e_C(A)$  can be used with high accuracy for heavy nuclei with  $X \neq 0$ .

Taking into account Eqs. (5), (8) and (12), we suggest the following new form for the  $\beta$ -stability line

$$X^*(A) = \frac{C_1 A^{2/3} + C_2 A^{1/3}}{C_1 A^{2/3} + C_2 A^{1/3} + b_V + b_S A^{-1/3}}. \quad (13)$$

Fitting  $X^*(A)$  in Fig. 1 by formula (13), we can derive the smooth "experimental" parameters of the symmetry energy  $b_V$  and  $b_S$ . The corresponding smooth behavior of  $X^*(A)$  is shown in Fig. 1 by solid thick line. This line was obtained as a best fit with the values of  $b_{\text{sym,vol}} = 27$  MeV and  $b_{\text{sym,surf}} = -23$  MeV which provide the surface-to-volume ratio  $r_{S/V} = |b_S|/b_V \approx 0.85$ . Note that the analysis made in Ref. [1] for the saddle point shapes of fissile nuclei gives the value for the surface symmetry coefficient of about  $b_S \approx -25$  MeV.

Approximating the contribution of the Coulomb energy to  $\Delta\lambda(A, X)$  by Eq. (12), one can extract  $b(A)$  at fixed neutron excess  $A_- \neq 0$  from the experimental values of  $\Delta\lambda$  by means of Eq. (9). We have performed such kind of numerical calculations of the "experimental" symmetry energy coefficient  $b(A)$  as a function of mass number  $A$  beyond the  $\beta$ -stability line for the values of the fixed neutron excess  $A_- = 18, 22, 26$  and  $30$ . The corresponding results are shown in Fig. 2. As seen from Fig. 2, qualitatively,  $b(A)$  has canyon-like behavior for a given value of  $A_-$ . Such kind of canyon-like behavior of the symmetry energy correlates with the nuclear subshell structure. The width and the position of the bottom for the "canyon" depend on the neutron excess  $A_-$ . The left wall of the canyon corresponds to the proton closed shell and the right wall corresponds to the neutron shell closure. Such kind of features can be understood from Eq. (9) and the fact that the value of the nucleon chemical potential  $\lambda_q$  goes up sharply when one moves from the closed shell to the one which is far from closure. In Fig. 2 the walls are located symmetrically with respect to  $A = 132$  which corresponds to both neutron and proton closed shell ( $N = 82$ ,  $Z = 50$ ). From  $A_- = 18$  to  $A_- = 30$  the shape of  $b(A)$  changes to thinner and deeper canyon with the local minimum in the symmetry coefficient being located at mass number which corresponds to double (proton-neutron) magic number. One can conclude that the thin canyon-like structure of the symmetry energy coefficient  $b(A)$  is caused by the shell effects in the single-particle level distribution near the nucleon Fermi energy.

## ISOSPIN EFFECTS WITHIN GIBBS – TOLMAN APPROACH

We consider first the spherical nucleus at zero temperature, having the mass number  $A = N + Z$ , the neutron excess  $A_- = N - Z$  and the asymmetry parameter  $X = A_-/A$ . The total binding energy of nucleus

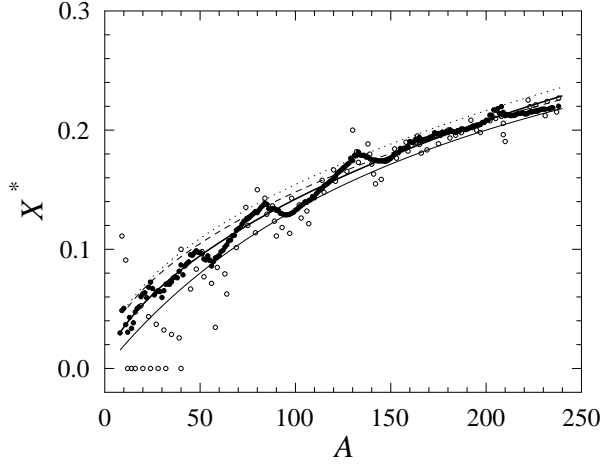


**Fig. 1:** Asymmetry parameter  $X^*(A)$  versus the mass number  $A$ . Solid dots represent the data obtained from the condition  $\Delta\lambda(A, X) = 0$ . Open circles correspond to the stable isotopes of maximum abundance for different elements. Solid lines present  $X^*(A)$  from Eq. (11) (thin) and from Eq. (13) with  $b_V = 27$  MeV,  $b_S = -23$  MeV (thick). The calculations using different Skyrme forces are shown by the dashed (SLy230b) and dotted (SkM) lines [30].

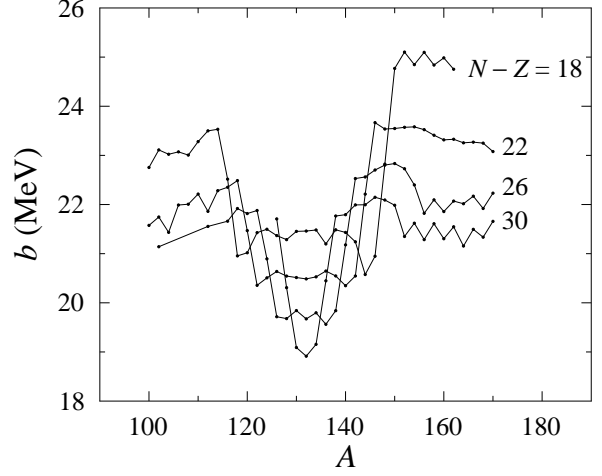


**Fig. 2:** The symmetry coefficient  $b$  vs mass number  $A$  at fixed neutron excess  $A_- = N - Z$ . The values of the neutron excess are specified by numbers near the curves.

is  $E$ . An actual nucleus has the finite diffuse layer of particle density distribution. Thereby, the nuclear size is badly specified. In order to formulate proper definition for the nuclear radius, we will use the concept of dividing surface of radius  $R$ , originally introduced by Gibbs [14]. Following Refs. [36, 14], we introduce the formal dividing surface of radius  $R$ , the corresponding volume  $V = 4\pi R^3/3$  and the surface area  $S = 4\pi R^2$ . Note that the dividing surface is arbitrary but it should be located within the nuclear diffuse layer.

The energy of a nucleus  $E$ , as well as the mass number  $A$  and the neutron excess  $A_-$ , are splitted into the volume and surface parts,

$$E = E_V + E_S + E_C, \quad A = A_V + A_S, \quad A_- = A_{-,V} + A_{-,S}. \quad (14)$$

Here the Coulomb energy  $E_C$  is fixed and does not depend on the dividing radius  $R$ . The bulk energy  $E_V$  and the surface energies  $E_S$  can be written as [17, 36]

$$E_V = (-P + \lambda \varrho_V + \lambda_- \varrho_{-,V}) V \quad \text{and} \quad E_S = (\sigma + \lambda \varrho_S + \lambda_- \varrho_{-,S}) S. \quad (15)$$

Here  $P$  is the bulk pressure

$$P = - \left. \frac{\partial E_V}{\partial V} \right|_{A_V}, \quad (16)$$

$\sigma$  is the surface tension and  $\varrho_V = A_V/V$  and  $\varrho_{-,V} = A_{-,V}/V$  are, respectively, the total (isoscalar) and the neutron excess (isovector) volume densities,  $\varrho_S = A_S/S$  and  $\varrho_{-,S} = A_{-,S}/S$  are the corresponding surface densities. We have used the isoscalar  $\lambda = (\lambda_n + \lambda_p)/2$  and isovector  $\lambda_- = (\lambda_n - \lambda_p)/2$  chemical potentials, where  $\lambda_n$  and  $\lambda_p$  are the chemical potentials of neutron and proton, respectively. The Coulomb energy  $E_C$  must be excluded from the chemical potentials  $\lambda$  and  $\lambda_-$  because of Eqs. (14) and (15). Namely,

$$\lambda_n = \left. \frac{\partial E}{\partial N} \right|_Z, \quad \lambda_p = \left. \frac{\partial E}{\partial Z} \right|_N - \lambda_C, \quad \text{where} \quad \lambda_C = \left. \frac{\partial E_C}{\partial Z} \right|_N. \quad (17)$$

Note that the definition of  $\lambda_p$  in Eq. (17) differs from the previous one given by (3). Notation  $E_V$  stands for the nuclear matter energy of the uniform densities  $\varrho_V$ ,  $\varrho_{-,V}$  within the volume  $V$ . The state of the nuclear matter inside the specified volume  $V$  is chosen to have the chemical potentials  $\mu$  and  $\mu_-$  equal to that of the actual droplet. In more detail, from the equation of state for the nuclear matter one has chemical potentials

$\mu(\rho, \rho_-)$  and  $\mu_-(\rho, \rho_-)$  as functions of the isoscalar,  $\rho$ , and isovector,  $\rho_-$ , densities. Then, the following conditions should be fulfilled:

$$\mu(\rho = \varrho_V, \rho_- = \varrho_{-,V}) = \lambda, \quad \mu_-(\rho = \varrho_V, \rho_- = \varrho_{-,V}) = \lambda_- \quad (18)$$

to derive the specific values of densities  $\varrho_V$  and  $\varrho_{-,V}$ .

The surface part of the energy  $E_S$  as well as the surface particle number  $A_S$  and the surface neutron excess  $A_{-,S}$  are considered as the excess quantities responsible for “edge” effects with respect to the corresponding volume quantities. Using Eqs. (14), (15) one obtains

$$\sigma = \frac{E - \lambda A - \lambda_- A_-}{S} + \frac{PV}{S} - \frac{E_C}{S} = \frac{\Omega - \Omega_V}{S}. \quad (19)$$

Here the grand potential  $\Omega = E - \lambda A - \lambda_- A_- - E_C$  and its volume part  $\Omega_V = -PV = E_V - \lambda A_V - \lambda_- A_{-,V}$  were introduced. From Eq. (19) one can see how the value of the surface tension depends on the choice of the dividing radius  $R$ ,

$$\sigma[R] = \frac{\Omega}{4\pi R^2} + \frac{1}{3}PR. \quad (20)$$

Taking the derivative from Eq. (20) with respect to the formal dividing radius  $R$  and using the fact that observables  $E$ ,  $\lambda$ ,  $\lambda_-$  and  $P$  should not depend on the choice of the dividing radius, one can rewrite Eq. (20) as

$$P = 2 \frac{\sigma[R]}{R} + \frac{\partial}{\partial R} \sigma[R], \quad (21)$$

which is the generalized Laplace equation. The formal values of surface densities  $\varrho_S$  and  $\varrho_{-,S}$  can be found from (14) as

$$\varrho_S[R] = \frac{A}{4\pi R^2} - \frac{1}{3}\varrho_V R, \quad \varrho_{-,S}[R] = \frac{A_-}{4\pi R^2} - \frac{1}{3}\varrho_{-,V} R. \quad (22)$$

In Eqs. (20) – (22) square brackets denote a formal dependence on the dividing radius  $R$  which is still arbitrary and may not correspond to the actual physical size of the nucleus. To derive the physical size quantity an additional condition should be imposed on the location of dividing surface. In general, the surface energy  $E_S$  for the arbitrary dividing surface includes the contributions from the surface tension  $\sigma$  and from the binding energy of particles within the surface layer. The latter contribution can be excluded for the special choice of dividing (equimolar) radius  $R = R_e$  which satisfy the condition

$$(\varrho_S \lambda + \varrho_{-,S} \lambda_-)_{R=R_e} = 0. \quad (23)$$

Here we use the notation  $R_e$  by the analogy with the equimolar dividing surface for the case of the one-component liquid [16, 36]. For the dividing radius defined by Eq. (23) the surface energy reads

$$E_S = \sigma_e S_e, \quad (24)$$

where  $\sigma_e \equiv \sigma(R_e)$  and  $S_e = 4\pi R_e^2$ . Using Eqs. (22), (23), the corresponding volume  $V_e = 4\pi R_e^3/3$  is written as

$$V_e = \frac{\lambda A + \lambda_- A_-}{\lambda \varrho_V + \lambda_- \varrho_{-,V}}. \quad (25)$$

As seen from Eqs. (18), (25), the droplet radius  $R_e$  is determined by the equation of state for the nuclear matter through the values of the droplet chemical potentials  $\lambda$  and  $\lambda_-$ .

The surface tension  $\sigma[R]$  depends on the location of the dividing surface. Function  $\sigma[R]$  has a minimum at certain radius  $R = R_s$  (radius of the surface of tension [36]) which usually does not coincide with the equimolar radius  $R_e$ . The radius  $R_s$  (Laplace radius) denotes the location within the interface. Note that for  $R = R_s$  the capillary pressure of Eq. (21) satisfies the classical Laplace relation

$$P = 2 \left. \frac{\sigma[R]}{R} \right|_{R=R_s}. \quad (26)$$

The dependence of the surface tension  $\sigma[R]$  of Eq. (20) on the location of the dividing surface for the nuclei  $^{120}\text{Sn}$  and  $^{208}\text{Pb}$  is shown in Fig. 3.

Following Gibbs and Tolman [14, 15], we will assume that the physical (measurable) value of the surface tension is that taken at the equimolar dividing surface. We assume, see also Ref. [36], that the surface tension  $\sigma \equiv \sigma(R_e)$  approaches the planar limit  $\sigma_\infty$  as

$$\sigma(R_e) = \sigma_\infty \left( 1 - \frac{2\xi}{R_e} + \mathcal{O}(R_e^{-2}) \right), \quad (27)$$

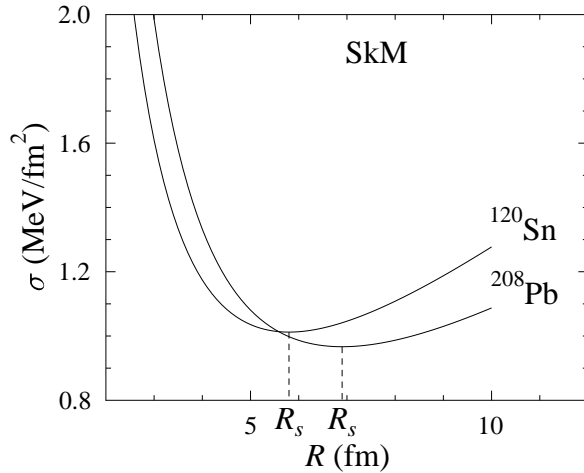


**Fig. 3:** Surface tension  $\sigma$  as a function of the dividing radius  $R$  for nuclei  $^{120}\text{Sn}$  and  $^{208}\text{Pb}$ . The calculation was performed using SkM force (see [37] for details). The Laplace radius  $R_s$  denotes the dividing radius where  $\sigma$  approaches the minimum value, i.e., the Laplace condition of Eq. (26) is satisfied.

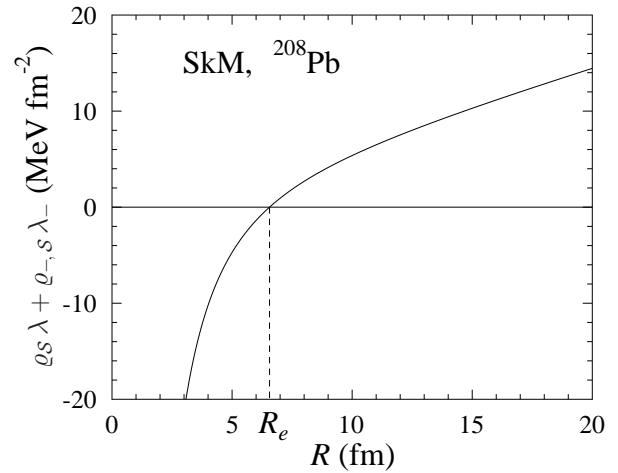


**Fig. 4:** Specific surface particle density  $\rho_S\lambda + \rho_{-,S}\lambda_-$  versus dividing radius  $R$  for  $^{208}\text{Pb}$ . The calculation was performed using the SkM force.  $R_e$  denotes the equimolar radius where  $\rho_S\lambda + \rho_{-,S}\lambda_-$  becomes zero.

where  $\xi$  is the Tolman's length [15]. Taking Eq. (21) for  $R = R_s$  and comparing with analogous one for  $R = R_e$ , one can establish the following important relation (see Eq. (45) in the next Section)

$$\xi = \lim_{A \rightarrow \infty} (R_e - R_s) + \mathcal{O}(X^2). \quad (28)$$

This result leads to the conclusion that to obtain the non-zero value of Tolman length  $\xi$ , and, consequently, the curvature correction  $\Delta\sigma_{\text{curv}} \neq 0$  for a curved surface, the nucleus must have a finite diffuse surface layer.

We perform the numerical calculations using Skyrme type of the effective nucleon-nucleon interaction. The energy and the chemical potentials for actual droplets can be calculated using a direct variational method within the extended Thomas-Fermi approximation [18, 37]. Using obtained chemical potentials we evaluate the equilibrium bulk densities  $\rho_V$  and  $\rho_{-,V}$  from Eq. (18). For arbitrary dividing radius  $R$  and fixed asymmetry parameter  $X$  we evaluate then the volume,  $A_V = 4\pi\rho_V R^3/3$  and  $A_{-,V} = 4\pi\rho_{-,V} R^3/3$ , the surface,  $A_S = 4\pi\rho_S R^2$  and  $A_{-,S} = 4\pi\rho_{-,S} R^2$ , particle numbers and the volume part of equilibrium energy  $E_V$ . All evaluated values of  $E_V[R]$ , the bulk densities  $\rho_V$  and  $\rho_{-,V}$  and the surface particle densities  $\rho_S[R]$  and  $\rho_{-,S}[R]$  depend on the radius  $R$  of dividing surface and asymmetry parameter  $X$ . The actual physical radius  $R_e$  of the droplet can be derived by the condition (23), i.e., by the requirements that the contribution to  $E_S$  from the bulk binding energy (term  $\sim (\rho_S\lambda + \rho_{-,S}\lambda_-)$  in Eq. (15)) should be excluded from the surface energy  $E_S$ . In Fig. 4 we represent the calculation of the specific surface particle density  $\rho_S\lambda + \rho_{-,S}\lambda_-$  as a function of the radius  $R$  of dividing surface. Equimolar dividing radius  $R_e$  in Fig. 4 defines the physical size of the sharp surface droplet and the surface at which the surface tension is applied, i.e., the equimolar surface where Eq. (24) is fulfilled.

Note that the value of equimolar radius  $R_e$ , which is derived by Eq. (25), is not considerably affected by the Coulomb interaction. We have also evaluated the values of  $R_e$  neglecting the Coulomb term, i.e., assuming  $E_C = \lambda_C = 0$ . The difference as compared with data obtained with Coulomb term included does not exceed 0.5% for  $A$  of about 200. Omitting the Coulomb energy contribution to the total energy  $E$  and evaluating the bulk energy  $E_V$ , one can obtain the surface part of energy  $E_S = E - E_V$  and the surface tension coefficient  $\sigma(R_e)$  (19) at the equimolar dividing surface for nuclei with different mass number  $A \propto R_e^3$  and asymmetry parameter  $X$ . The dependence of the surface tension coefficient  $\sigma(R_e)$  on the doubled inverse equimolar radius  $2/R_e$  (see Eq. (27)) is shown in Fig. 5.

The surface tension  $\sigma(R_e, X)$  approaches the planar limit  $\sigma_\infty(X)$  in the limit of zero curvature  $2/R_e \rightarrow 0$ . As seen from Fig. 5, the planar limit  $\sigma_\infty(X)$  depends on the asymmetry parameter. This dependence reflects the fact that the symmetry energy  $b$  in mass formula contains both the volume  $b_V$  and surface  $b_S$  contributions, see Refs. [38, 29]. In Fig. 6 we show the  $X$ -dependence of the surface tension  $\sigma_\infty(X)$ . This dependence can be approximated by

$$\sigma_\infty(X) = \sigma_0 + \sigma_- X^2. \quad (29)$$

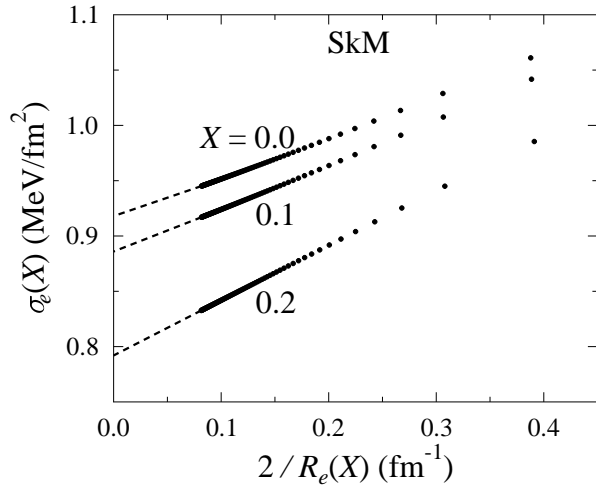


**Fig. 5:** The dependence of the surface tension coefficient  $\sigma(R_e, X)$  on the equimolar radius  $R_e$  for different values of the asymmetry parameter  $X$ . The calculation was performed for Skyrme force SkM [37].

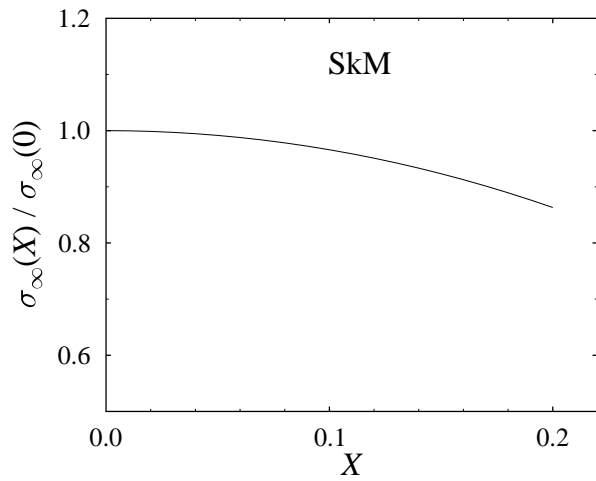


**Fig. 6:** Dependence of the planar surface tension  $\sigma_\infty(X)$  on the asymmetry parameter  $X$ . The calculation was performed for Skyrme force SkM.

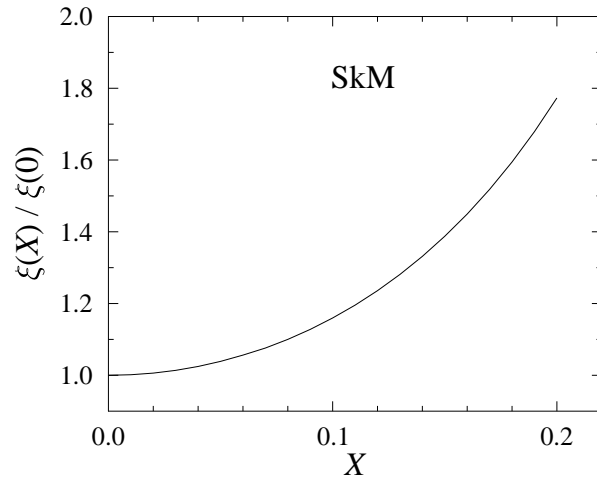


**Fig. 7:** Dependence of the Tolman length  $\xi$  on the asymmetry parameter  $X$ . The calculation was performed for Skyrme force SkM.

The dependence of parameters  $\sigma_0$  and  $\sigma_-$  on the Skyrme force parametrization is shown in Table 1. The isovector term  $\sigma_-$  in the surface tension (29) is related to the surface contribution  $b_S$  to the symmetry energy (see the next Section, Eq. (42)). We evaluate the surface-to-volume ratio  $r_{S/V} = |b_S/b_V| = 1.17 \div 1.47$  for Skyrme force parametrizations from Table 1. Note that in the previous theoretical calculations, the value of surface-to-volume ratio  $r_{S/V}$  varies strongly within the interval  $1.6 \leq r_{S/V} \leq 2.8$ , see Refs. [38, 29, 39].

The slope of curves  $\sigma(R_e)$  in Fig. 5 gives the Tolman length  $\xi$ , see Eq. (27). The value of the Tolman length  $\xi$  depends significantly on the asymmetry parameter  $X$ . In Fig. 7 we show such kind of dependence obtained from results of Fig. 5. As seen from Fig. 7, one can expect the enhancement of the curvature effects in neutron rich nuclei. The  $X$ -dependence of Tolman length  $\xi$  can be approximated as

$$\xi(X) = \xi_0 + \xi_- X^2. \quad (30)$$

Both parameters  $\xi_0$  and  $\xi_-$  as well as the surface tension parameter  $\sigma_-$  are rather sensitive to the Skyrme force parametrization, see Table 1.

## NUCLEAR MATTER EQUATION OF STATE AND $(A^{-1/3}, X)$ -EXPANSION FOR FINITE NUCLEI

We will consider the relation of the nuclear macroscopic characteristics (surface and symmetry energies, Tolman length, incompressibility, etc.) to the bulk properties of nuclear matter. Assuming a small deviations from the equilibrium, the equation of state (EOS) for an asymmetric nuclear matter can be written in the



form expansion around the saturation point. One has for the energy per particle (at zero temperature)

$$\mathcal{E}(\epsilon, x) = \frac{E_\infty}{A} = \mu_\infty + \frac{K_\infty}{18} \epsilon^2 + b_\infty x^2 + \dots, \quad (31)$$

where

$$\epsilon = \frac{\rho - \rho_\infty}{\rho_\infty}, \quad x = \frac{\rho_-}{\rho}, \quad \rho = \rho_n + \rho_p, \quad \rho_- = \rho_n - \rho_p,$$

$\rho_\infty$  is the matter saturation (equilibrium) density,  $\mu_\infty$  is the chemical potential,  $K_\infty$  is the nuclear matter incompressibility and  $b_\infty$  is the symmetry energy coefficient (all values are taken at the saturation point  $\epsilon = 0$  and  $x = 0$ ). Coefficients of expansion (31) are determined through the derivatives of the energy per particle  $\mathcal{E}(\epsilon, x)$  at the saturation point:

$$\mu_\infty = \left. \frac{E_\infty}{A} \right|_{\text{s.p.}} \equiv \mathcal{E}^{(0,0)}, \quad K_\infty = 9 \rho^2 \left. \frac{\partial^2 E_\infty / A}{\partial \rho^2} \right|_{\text{s.p.}} \equiv 9 \mathcal{E}^{(2,0)}, \quad b_\infty = \frac{1}{2} \left. \frac{\partial^2 E_\infty / A}{\partial x^2} \right|_{\text{s.p.}} \equiv \frac{1}{2} \mathcal{E}^{(0,2)}. \quad (32)$$

Here we use the short notations  $\text{s.p.} \equiv (\rho = \rho_\infty, x = 0)$  and  $\mathcal{E}^{(n,m)} \equiv \left. \frac{\partial^{n+m} \mathcal{E}}{\partial \epsilon^n \partial x^m} \right|_{\epsilon=0, x=0}$ . Some coefficients  $\mathcal{E}^{(n,m)}$  are vanishing. From the condition of minimum of  $\mathcal{E}(\epsilon, x)$  at the saturation point one has  $\mathcal{E}^{(1,0)} = \mathcal{E}^{(0,1)} = 0$ . Odd derivatives with respect to  $x$ , i.e.,  $\mathcal{E}^{(n,m)}$  for odd  $m$ , also vanish because of the charge symmetry of nuclear forces. Using  $\mathcal{E}(\epsilon, x)$ , one can also evaluate chemical potentials  $\mu$ ,  $\mu_-$  and pressure  $P$  of the nuclear matter beyond the saturation point. Namely,

$$\mu(\epsilon, x) = \left. \frac{\partial E_\infty}{\partial A} \right|_{A_-, V} = \frac{\partial}{\partial \epsilon} (1 + \epsilon) \mathcal{E} - x \frac{\partial \mathcal{E}}{\partial x}, \quad \mu_-(\epsilon, x) = \left. \frac{\partial E_\infty}{\partial A_-} \right|_{A, V} = \frac{\partial \mathcal{E}}{\partial x}, \quad (33)$$

$$P(\epsilon, x) = - \left. \frac{\partial E_\infty}{\partial V} \right|_{A, A_-} = \rho_\infty (1 + \epsilon)^2 \frac{\partial \mathcal{E}}{\partial \epsilon}. \quad (34)$$

Similarly to Eq. (31), in a finite uncharged system the energy per particle  $E/A$  (we use  $A = N + Z$ ,  $A_- = N - Z$ ,  $X = A_-/A$ ) of the finite droplet is usually presented as  $(A^{-1/3}, X)$ -expansion around infinite matter using the leptodermous approximation

$$E/A = a_V + a_S A^{-1/3} + a_C A^{-2/3} + X^2 (b_V + b_S A^{-1/3} + b_C A^{-2/3}) \quad (35)$$

where  $a_V$ ,  $a_S$  and  $a_C$  are, respectively, the volume, surface and curvature energy coefficients,  $b_V$ ,  $b_S$  and  $b_C$  are, respectively, the volume, surface and curvature symmetry coefficients. The nuclear chemical potentials  $\lambda$  and  $\lambda_-$  are derived as

$$\lambda(X, A^{-1/3}) = E/A - \frac{1}{3} A^{-1/3} \frac{\partial E/A}{\partial A^{-1/3}} - X \frac{\partial E/A}{\partial X}, \quad \lambda_-(X, A^{-1/3}) = \frac{\partial E/A}{\partial X}. \quad (36)$$

Following Gibbs-Tolman method, one can derive the actual nuclear matter densities  $\rho$  and  $\rho_-$  from the conditions

$$\mu(\epsilon, x) = \lambda(X, A^{-1/3}), \quad \mu_-(\epsilon, x) = \lambda_-(X, A^{-1/3}). \quad (37)$$

Using Eq. (37), one can establish the relation of the macroscopic energy coefficients in the mass formula expansion Eq. (35) to the nuclear matter parameters in EOS (31), see Eqs. (41) – (45) below. The results of numerical calculations of relevant quantities are represented in Tables 1 and 2.

We start from the nuclear matter EOS given by Eq. (31) and take into consideration the relations (32) and the following higher order coefficients

$$K_3 = 6K_\infty + 27 \rho^3 \left. \frac{\partial^3 E_\infty / A}{\partial \rho^3} \right|_{\text{s.p.}} \equiv 27 (\mathcal{E}^{(3,0)} + 2 \mathcal{E}^{(2,0)}), \quad L_\infty = \frac{3}{2} \rho \left. \frac{\partial^3 E_\infty / A}{\partial \rho \partial x^2} \right|_{\text{s.p.}} \equiv \frac{3}{2} \mathcal{E}^{(1,2)}, \quad (38)$$

$$K_{\text{sym}} = \frac{9}{2} \rho^2 \left. \frac{\partial^4 E_\infty / A}{\partial \rho^2 \partial x^2} \right|_{\text{s.p.}} \equiv \frac{9}{2} \mathcal{E}^{(2,2)}, \quad (39)$$

for the expansion (31). Here  $K_3$  is the bulk anharmonicity coefficient,  $L_\infty$  is the density-symmetry coefficient (symmetry energy slope parameter),  $K_{\text{sym}}$  is the symmetry energy curvature parameter. Using (27), we write also

$$\sigma \approx \sigma_\infty (1 - 2\xi/R_e), \quad \sigma_\infty \approx \sigma_0 + \sigma_- X^2, \quad \xi \approx \xi_0 + \xi_- X^2, \quad (40)$$

and, taking the advantage of the large mass limit  $E_\infty/A = E/A|_{X=\text{const}, A \rightarrow \infty}$ , one has

$$a_V = \mu_\infty, \quad b_V = b_\infty. \quad (41)$$

Using the conditions (37) for the chemical potentials and both relations (36) and (33), we obtain  $\rho/\rho_\infty \approx 1 + 6A^{-1/3}a_S/K_\infty - 3X^2L_\infty/K_\infty$  and

$$a_S = 4\pi r_0^2 \sigma_0, \quad b_S = 4\pi r_0^2 \left( \sigma_- + \frac{2L_\infty}{K_\infty} \sigma_0 \right), \quad a_c = -8\pi r_0 \sigma_0 \left( \xi_0 + \frac{3\sigma_0}{K_\infty \rho_\infty} \right), \quad (42)$$

$$b_c = -8\pi r_0 \sigma_0 \left\{ \xi_- + \left( \frac{L_\infty}{K_\infty} + \frac{\sigma_-}{\sigma_0} \right) \xi_0 + \frac{3\sigma_0}{K_\infty \rho_\infty} \left[ \frac{L_\infty}{K_\infty} \left( 4 + \frac{K_3}{K_\infty} \right) - \frac{K_{\text{sym}}}{K_\infty} \right] + \frac{3\sigma_-}{K_\infty \rho_\infty} \left( 2 + \frac{K_\infty \sigma_-}{2b_\infty \sigma_0} \right) \right\}.$$

Here  $r_0 = (4\pi\rho_\infty/3)^{-1/3}$  and we have assumed  $A^{-1/3} \ll 1$ . The equimolar,  $R_e$ , and Laplace,  $R_s$ , radii defined by Eqs. (25) and (26) read

$$R_e \approx r_0 A^{1/3} \left[ 1 - A^{-1/3} \frac{8\pi r_0^2 \sigma_0}{K_\infty} + X^2 \left[ \frac{L_\infty}{K_\infty} - A^{-1/3} \left\{ \frac{8\pi r_0^2 \sigma_-}{K_\infty} \left( 1 - \frac{L_\infty}{b_\infty} + \frac{K_\infty}{3\mu_\infty} \right) + \frac{8\pi r_0^2 \sigma_0}{K_\infty} \left[ \frac{L_\infty}{K_\infty} \left( 3 + \frac{K_3}{K_\infty} \right) - \frac{K_{\text{sym}}}{K_\infty} \right] \right\} \right] \right], \quad (43)$$

$$R_s \approx r_0 A^{1/3} \left[ 1 - A^{-1/3} \left( \frac{\xi_0}{r_0} + \frac{8\pi r_0^2 \sigma_0}{K_\infty} \right) + X^2 \left[ \frac{L_\infty}{K_\infty} - A^{-1/3} \left\{ \frac{\xi_-}{r_0} + \frac{8\pi r_0^2 \sigma_-}{K_\infty} \left( 1 + \frac{K_\infty \sigma_-}{2b_\infty \sigma_0} \right) + \frac{8\pi r_0^2 \sigma_0}{K_\infty} \left[ \frac{L_\infty}{K_\infty} \left( 3 + \frac{K_3}{K_\infty} \right) - \frac{K_{\text{sym}}}{K_\infty} \right] \right\} \right] \right]. \quad (44)$$

Using the derivations of  $R_e$  and  $R_s$ , one obtains

$$R_e - R_s \approx \xi_0 + \left[ \xi_- + \frac{3\sigma_-}{b_\infty \rho_\infty} \left( \frac{\sigma_-}{\sigma_0} + \frac{2L_\infty}{K_\infty} - \frac{2b_\infty}{3\mu_\infty} \right) \right] X^2 = \xi + \left[ \frac{3\sigma_-}{b_\infty \rho_\infty} \left( \frac{\sigma_-}{\sigma_0} + \frac{2L_\infty}{K_\infty} - \frac{2b_\infty}{3\mu_\infty} \right) \right] X^2. \quad (45)$$

To describe separately the neutron and proton density distributions we introduce the neutron radius,  $R_n$ , and the proton radius,  $R_p$ , as the dividing radii with zero value for the corresponding surface densities  $\varrho_{n,S} = (\varrho_S + \varrho_{-,S})/2$  and  $\varrho_{p,S} = (\varrho_S - \varrho_{-,S})/2$ :

$$\varrho_{n,S}|_{R=R_n} = 0, \quad \varrho_{p,S}|_{R=R_p} = 0.$$

The isovector shift of neutron-proton radii,  $R_n - R_p$ , is then written as

$$R_n - R_p \approx X \left[ -\frac{2\sigma_-}{b_\infty \rho_\infty} + A^{-1/3} \left\{ 4\pi r_0^2 \sigma_0 \frac{4}{3b_\infty} \left( \xi_- + \xi_0 \frac{\sigma_-}{\sigma_0} \right) + 4\pi r_0^2 \sigma_- \left[ \frac{2\sigma_-}{b_\infty^2 \rho_\infty} + \frac{4\sigma_0}{b_\infty^2 \rho_\infty} \left( \frac{L_\infty}{K_\infty} + \frac{3b_\infty}{K_\infty} \right) \right] \right\} \right]. \quad (46)$$

From Eq. (46) the value of neutron skin  $\sqrt{\langle r_n^2 \rangle} - \sqrt{\langle r_p^2 \rangle}$  is given within the main order as

$$\sqrt{\langle r_n^2 \rangle} - \sqrt{\langle r_p^2 \rangle} \approx -\sqrt{\frac{3}{5}} \frac{2\sigma_- X}{b_\infty \rho_\infty} = \alpha X. \quad (47)$$

Here  $\alpha = -2\sqrt{3/5}\sigma_-/(b_\infty \rho_\infty)$  is the neutron skin parameter. To describe the isospin dependence of surface energy within the droplet model the effective surface stiffness,  $Q$ , have been introduced [19]. At the large masses limit  $A \rightarrow \infty$  the droplet model result reads

$$R_n - R_p \approx \frac{3}{2} r_0 \frac{b_\infty}{Q} X. \quad (48)$$

Using the main term on the right side of Eq. (46) together with Eq. (48) one obtains the surface stiffness  $Q$  as

$$Q = -\frac{9b_\infty^2}{16\pi r_0^2 \sigma_-}. \quad (49)$$

The values of  $\alpha$  and  $Q$  for different Skyrme forces are given in Table 3.

**Tab. 1:** Nuclear bulk parameters for different Skyrme forces. The planar surface values  $\sigma_0$ ,  $\sigma_-$  and  $\xi_0$ ,  $\xi_-$  were obtained by extrapolation  $A \rightarrow \infty$ , see Fig. 5.

	SkM	SkM*	SLy230b	T6
$\mu_\infty$ (MeV)	-15.77	-15.77	-15.97	-15.96
$\rho_\infty$ (fm $^{-3}$ )	0.1603	0.1603	0.1595	0.1609
$K_\infty$ (MeV)	216.6	216.6	229.9	235.9
$K_3$ (MeV)	913.5	913.5	1016.	1032.
$K_{\text{sym}}$ (MeV)	-148.8	-155.9	-119.7	-211.5
$b_\infty$ (MeV)	30.75	30.03	32.01	29.97
$L_\infty$ (MeV)	49.34	45.78	45.97	30.86
$\sigma_0$ (MeV/fm $^2$ )	0.9176	0.9601	1.006	1.021
$\xi_0$ (fm)	-0.3565	-0.3703	-0.3677	-0.3593
$\sigma_-$ (MeV/fm $^2$ )	-3.118	-3.094	-3.131	-2.413
$\xi_-$ (fm)	-5.373	-5.163	-4.590	-2.944

**Tab. 2:** Mass formula coefficients for finite nuclei.

	SkM	SkM*	SLy230b	T6
$a_V$ (MeV)	-15.8	-15.8	-16.0	-16.0
$a_S$ (MeV)	15.0	15.7	16.5	16.7
$a_c$ (MeV)	7.30	7.92	8.26	8.16
$b_V$ (MeV)	30.8	30.0	32.0	30.0
$b_S$ (MeV)	-44.2	-44.1	-44.9	-35.1
$b_c$ (MeV)	35.7	35.1	28.6	17.3
$r_{S/V} =  b_S/b_V $	1.44	1.47	1.40	1.17

**Tab. 3:** Neutron skin parameter  $\alpha$  and surface stiffness  $Q$  for different Skyrme forces. The values of  $\alpha$  and  $Q$  were calculated using Eqs. (47) and (49), respectively.

	SkM	SkM*	SLy230b	T6
$\alpha$ (fm)	0.980	0.996	0.950	0.775
$Q$ (MeV)	41.6	40.0	44.8	51.2

## CONCLUSIONS

We propose a new method of the evaluation of the  $A$ -dependency of  $\beta$ -stability line and both the Coulomb,  $e_C(A)$ , and the symmetry,  $b(A)$ , energies. Our method is model independent in a sense that it does not imply a theoretical model for the calculation of the nuclear binding energy. The method is based on the experimental data for the shift of the neutron-proton chemical potential  $\Delta\lambda(A, X)$  for nuclei beyond  $\beta$ -stability line but at the fixed total particle number  $A$ . We show the presence of the thin structure (sawtooth shape) of  $\beta$ -stability line for the curve  $X^*(A)$  which is not observed at the traditional presentation of  $\beta$ -stability line as  $Z(N)$ -dependency. We note that this non-monotonic behavior of  $\beta$ -stability line is the consequence of subshell structure of single particle levels near Fermi energy for both the neutrons and the protons. We demonstrate the correlation between the positions of maxima of function  $X^*(A)$  and double magic nucleon numbers.

We have suggested the model independent method for calculation of the Coulomb energy parameter  $e_C(A)$  which absorbs both the finite diffuse layer and the quantum exchange contributions. The last fact leads to more complicate  $A$ -dependence of  $e_C(A)$  (see Eq. (12)) than the traditional one  $e_C(A) \propto A^{2/3}$ . We have established the dependence of  $\beta$ -stability line  $X^*(A)$  on the Coulomb,  $e_C(A)$ , and the symmetry,  $b(A)$ , energies. That allowed us to redefine a smooth  $A$ -dependency of  $\beta$ -stability line (see Eq. (13)) which can be used instead the phenomenological one (11) given by Green and Engler [31]. One should note that it is difficult to determine  $b_V$  unambiguously. The reason is that the surface contribution cannot be neglected even for the heavy nuclei covered by the experimental data. Another reason is the different  $A$ -dependence for  $b(A)$  used in the nuclear mass formula, see e.g. Ref. [38].

We have also observed the thin structure of the symmetry energy  $b(A)$ . The value of  $b(A)$  has the canyon-like  $A$ -dependence for a fixed neutron excess  $A_- = N - Z$ . The width and the position of bottom for such a canyon-like shape depend on the neutron excess and are related to the subshell structure in the discrete spectrum of the single particle levels for both the neutrons and the protons. The canyon shape of  $b(A)$  becomes thinner and deeper near double (proton-neutron) magic number.

Considering a small two-component, charged droplet with a finite diffuse layer, we have introduced a formal dividing surface of radius  $R$  which splits the droplet onto volume and surface parts. The corresponding splitting was also done for the binding energy  $E$ . Assuming that the dividing surface is located close to the interface, we are then able to derive the surface energy  $E_S$ . In general, the surface energy  $E_S$  includes the contributions from the surface tension  $\sigma$  and from the binding energy of  $A_S$  particles located within the surface layer. The equimolar surface and thereby the actual physical size of the droplet are derived by the condition  $\varrho_S \lambda + \varrho_{-,S} \lambda_- = 0$  which means that the latter contribution is excluded from the surface energy providing  $E_S \propto \sigma$ .

In a small nucleus, the diffuse layer and the curved interface affect the surface properties significantly. In agreement with Gibbs-Tolman concept [15, 14], two different radii have to be introduced in this case. The

first radius,  $R_s$ , is the surface tension radius (Laplace radius) which provides the minimum of the surface tension coefficient  $\sigma$  and the fulfillment of the Laplace relation (26) for capillary pressure. The another one,  $R_e$ , is the equimolar radius which corresponds to the equimolar dividing surface due to the condition (23) and defines the physical size of the sharp surface droplet, i.e., the surface at which the surface tension is applied. The difference of two radii  $R_e - R_s$  in an asymptotic limit of large system  $A \rightarrow \infty$  derives the Tolman length  $\xi$ . That means the presence of curved surface is not sufficient for the presence of the curvature correction in the surface tension. The finite diffuse layer in the particle distribution is also required. We point out that the Gibbs–Tolman theory allows to treat a liquid drop within thermodynamics with minimum assumptions. Once the binding energy and chemical potential of the nucleus are known its equimolar radius, radius of tension and surface energy can be evaluated using the equation of state for the infinite nuclear matter. We have also established the relation of the macroscopic energy coefficients in the liquid drop model expansion Eq. (35) to the nuclear matter parameters.

The sign and the magnitude of the Tolman length  $\xi$  depend on the interparticle interaction. We have shown that the Tolman length is negative for a nuclear Fermi liquid drop. As a consequence, the curvature correction to the surface tension leads to the hindrance of the yield of light fragments at the nuclear multi-fragmentation in heavy ion collisions. We have also shown that the Tolman length is sensitive to the neutron excess and its absolute value growth significantly with growing asymmetry parameter  $X$ .

## REFERENCES

- [1] A. Bohr and B. Mottelson, *Nuclear Structure* (W.A. Benjamin, New York, 1975), Vol. II.
- [2] M.B. Tsang, W.A. Friedman, C.K. Gelbke, *et al.*, Phys. Rev. Lett. **86** (2001) 5023.
- [3] W.A. Friedman, Phys. Rev. C **69** (2004) 031601(R).
- [4] M. Veselsky, G.A. Souliotis, and M. Jandel, Phys. Rev. C **69** (2004) 044607.
- [5] T.X. Liu, X.D. Liu, M.J. van Goethem, W.G. Lynch, *et al.*, Phys. Rev. C **69** (2004) 014603.
- [6] G.A. Souliotis, D.V. Shetty, M. Veselsky, *et al.*, Phys. Rev. C **68** (2003) 024605.
- [7] M. Veselsky, G.A. Souliotis, and S.J. Yennello, Phys. Rev. C **69** (2004) 031602(R).
- [8] E. Geraci, M. Bruno, M. D’Agostino, E. De Filippo, *et al.*, Nucl. Phys. **A732** (2004) 173.
- [9] Y.G. Ma, K. Wang, X.Z. Cai, J.G. Chen, *et al.*, Phys. Rev. C **72** (2005) 064603.
- [10] G. Audi, A.H. Wapstra and C. Thibault, Nucl. Phys. **A729** (2003) 337.
- [11] J. Jänecke, T.W. O’Donnell and V.I. Goldanskii, Nucl. Phys. **A728** (2003) 23.
- [12] W.E. Ormand, Phys. Rev. C **55** (1997) 2407.
- [13] M. Liu, N. Wang, Y. Deng and X. Wu, Phys. Rev. C **84** (2011) 014333.
- [14] J.W. Gibbs, in *The Collected Works* (Longmans, Green and Co., New York, 1928), Vol. I, p. 219.
- [15] R.C. Tolman, J. Chem. Phys. **17**, 118, 333 (1949).
- [16] V.M. Kolomietz, S.V. Lukyanov and A.I. Sanzhur, Phys. Rev. C **86** (2012) 024304.
- [17] L.D. Landau and E.M. Lifshitz, *Statistical Physics* (Pergamon Press, Oxford, 1958).
- [18] V.M. Kolomietz and A.I. Sanzhur, Eur. Phys. J. **38**, 345 (2008).
- [19] W.D. Myers and W.J. Swiatecki, Ann. Phys. (NY) **55**, 395 (1969).
- [20] W.D. Myers, W.J. Swiatecki and C.S. Wang, Nucl. Phys. **A 436**, 185 (1985).
- [21] M. Centelles, M. Del Estal and X. Viñas, Nucl. Phys. **A 635**, 193 (1998).
- [22] M. Centelles, X. Roca-Maza, X. Viñas and M. Warda, Phys. Rev. C **82** 054314 (2010).
- [23] X. Roca-Maza, M. Centelles, X. Viñas and M. Warda, Phys. Rev. Lett. **106** 252501 (2011).
- [24] J.M. Lattimer, C.J. Pethick, D.G. Ravenhall and D.Q. Lamb, Nucl. Phys. **A 432**, 646 (1985).
- [25] M. Brack, C. Guet and H.-B. Håkansson, Phys. Rep. **123**, 275 (1985).
- [26] M. Centelles and X. Viñas, Nucl. Phys. **A 563**, 173 (1993).
- [27] J. Treiner and H. Krivine, Ann. Phys. (NY) **170**, 406 (1986).
- [28] K. Kolehmainen, M. Prakash, J.M. Lattimer and J. Treiner, Nucl. Phys. **A 439**, 535 (1985).
- [29] V.M. Kolomietz and A.I. Sanzhur, Phys. Rev. C **81** (2010) 024324.
- [30] V.M. Kolomietz and A.I. Sanzhur, Int. J. Mod. Phys. E **22** (2013) 135003.
- [31] A.E.S. Green and N.A. Engler, Phys. Rev. **91** (1953) 40.
- [32] A. Bohr and B. R. Mottelson, *Nuclear Structure* (W.A. Benjamin, New York, 1969), Vol. 1.
- [33] V.M. Kolomietz, S.V. Lukyanov and A.I. Sanzhur, Phys. Rev. C **85** (2012) 034309.
- [34] K. Oyamatsu, I. Tanichata, S. Sugahara, K. Sumiyoshi and H. Toki, Nucl. Phys. **A634** (1998) 3.
- [35] K. Oyamatsu and K. Iida, Progr. Theor. Phys. **109** (2003) 631.
- [36] J.S. Rowlinson and B. Widom, *Molecular Theory of Capillarity* (Clarendon Press, Oxford, 1982).
- [37] V.M. Kolomietz and A.I. Sanzhur, Phys. Rev. C **88**, 044316 (2013).
- [38] P. Danielewicz, Nucl. Phys. **A727** (2003) 233.
- [39] W. Satuła, R.A. Wyss and M. Rafalski, Phys. Rev. C **74**, 011301(R) (2006).